PHYSICAL REVIEW C VOLUME 40, NUMBER 3 SEPTEMBER 1989

Relativistic Hartree calculations of odd-A nuclei

R. J. Furnstahl
Department of Physics and Astronomy, University of Maryland, College Park, Maryland 20742

C. E. Price*
Physics Division, Argonne National Laboratory, Argonne, Illinois 60439
and Department of Physics, University of Colorado, Boulder, Colorado 80309
(Received 23 January 1989)

Ground-state properties of odd-A nuclei near closed shells are calculated using self-consistent, relativistic mean-field models of baryon-meson dynamics. Contributions from σ, ω, and ρ mesons and the photon are included. Comparisons are made between linear and nonlinear mean-field models, and with calculations including vacuum polarization in a local density approximation. Results are given for (intrinsic) binding energies, rms radii, magnetic and quadrupole moments, currents, and elastic magnetic scattering form factors, with comparisons to other calculations and to experiment. Bulk systematics are well reproduced by the nonlinear model and, as expected, isoscalar magnetic moments in light nuclei are close to Schmidt predictions for all models. At higher momentum transfer, currents are enhanced compared to nonrelativistic single-particle predictions, in disagreement with experiment. Extensions to include pions and derivative corrections to the vacuum polarization current are discussed.

I. INTRODUCTION

Relativistic mean-field models have been successfully applied to a variety of problems in nuclear structure and nuclear reactions.[1] Early calculations showed that ground-state properties of spherical nuclei are well described in a mean-field model that is adjusted to reproduce empirical nuclear saturation properties.[2,3] Specifically, these models naturally generate the spin-orbit splitting that creates the nuclear shell structure, and make quantitatively accurate predictions of rms radii and charge densities. Furthermore, if nonlinear scalar meson couplings are included,[4] the resulting "best fit" to spherical nuclei is comparable to that achieved with nonrelativistic Skyrme models.[5] Finally, the ground-state densities provided by these structure calculations can be used as input to relativistic impulse-approximation calculations of polarized proton-nucleus scattering. The predictions for the spin observables from these simple calculations are in striking agreement with experimental results.[6]

Thus, relativistic mean-field models provide a simple and compelling phenomenology for nuclear structure physics. Although the Hartree (mean-field) approximation is best motivated for closed-shell nuclei, the models have been applied more widely, testing the mean-field phenomenology. Recent calculations show that models with nonlinear couplings can describe the deformation properties of even-even nuclei throughout the Periodic Table.[7–11] In this paper, we extend the deformed nucleus calculations further, to odd-A nuclei.[12–17] We emphasize the simplicity of the mean-field description; in this spirit, we proceed as far as possible without considering angular momentum projection, pairing, or higher-order corrections.

One early failure of relativistic mean-field models was the calculation of isoscalar magnetic moments for nuclei one particle or hole away from a closed shell.[2] These calculations used the simplest shell-model picture, in which the closed-shell core remains spherical and the valence nucleon determines the magnetic moment. With nonrelativistic wave functions, this approximation produces the well-known "Schmidt lines." In relativistic models, however, the reduced nucleon effective mass M^* in the nuclear medium (due to the large scalar field) results in a single-particle convection current enhanced by M/M^* compared to the nonrelativistic current, leading to sharp deviations from the isoscalar Schmidt predictions.

Experimentally, the *isoscalar* magnetic moments of LS closed-shell ± 1 nuclei are in reasonable agreement with the Schmidt values.[18] The disagreement between relativistic predictions and the experimental moments, in contrast to the successful nonrelativistic predictions, appeared to be an unwelcome signature of the large relativistic potentials. This "magnetic moment problem" of relativistic models has been the subject of much study during the past few years. The resolution of the problem is that the simple shell-model picture (or "impulse approximation") provides a poor approximation to the current of the self-consistent Hartree ground state for the odd-A system. The valence nucleon is a source of new meson fields, and the response of the core nucleons to these new fields cannot be neglected when computing the current. In nuclear matter calculations, the core wave functions are mixed with negative-energy states and the enhancement of the convection current is essentially canceled.[19–24] When this core response is applied to finite nuclei using a local density approximation, the result is a return to the isoscalar Schmidt moments.[23,24]

There are two paths to self-consistency in a full finite-nucleus calculation. One approach is to start with the basis of the spherical core nucleus (which is easily calculated) and to include the core response to the valence nucleon in a linear response approximation [random-phase approximation (RPA) ring sum].[25–28] Alternatively, one can consider the core plus valence system as a whole, treating all nucleons democratically, and then solve the Hartree equations for the (deformed) odd-A system directly. This is the approach we adopt in this paper. Note that the RPA is only an approximation to the fully self-consistent solution; the valence nucleon is treated as an *external* source of meson fields so that the core response does not act back on the valence wave function. This additional self-consistency is essentially a $1/A$ correction; in nuclear matter the RPA and self-consistent approaches are equivalent. The relationship between the two is discussed in detail in Refs. 23 and 26.

RPA calculations for finite nuclei in mean-field models have explicitly demonstrated that the convection current in a finite nucleus is constrained at low momentum transfer q to be close to nonrelativistic predictions (at least in LS closed shell ± 1 nuclei).[26–28] However, the current at higher q remains sensitive to the relativistic dynamics and becomes further enhanced by the core response. In this paper, self-consistent odd-A calculations verify the RPA results obtained in Refs. 25–28 for magnetic moments and currents, and extend them to additional nuclei.

Most of the calculations in this paper (and those in Refs. 25–27) are for the mean-field theory (MFT), which neglects contributions to the nucleon self-energy from the negative-energy Dirac sea (although negative-energy states contribute to the MFT/RPA response, as discussed above). RPA calculations have also been performed in the relativistic Hartree approximation (or RHA), which includes the effects of mean fields on the states in the Dirac sea.[28] Vacuum effects in the RHA dramatically change the nature of the core response at moderate momentum transfers (compared to the mean-field approximation) and may provide a more consistent treatment of convection currents.[29] In this paper, we consider part of the RHA physics through self-consistent calculations of odd-A nuclei that include vacuum polarization contributions in a local density approximation. A complete description would include the screening of the valence current from $N\bar{N}$ excitations, which appears as a nonzero vacuum polarization current in our self-consistent approach. This current can be calculated using a derivative expansion (as indicated in Sec. II C).

The outline of the paper is as follows. In Sec. II, we briefly review the relativistic Hartree formalism, emphasizing the new features in calculations of odd-A nuclei. In Sec. III, we present results for a wide range of nuclei, both in the σ-ω model, to compare to previous RPA calculations, and in models including the ρ meson and the photon (both linear and nonlinear). Calculated binding energies, rms radii, magnetic and quadrupole moments, and elastic magnetic scattering form factors are given. These results are discussed further in Sec. IV and our conclusions are summarized in Sec. V. Additional details of the calculated procedure are summarized in the Appendix.

II. FORMALISM

A. Walecka model

We begin with the Walecka (σ-ω) model including scalar meson self-couplings. The Lagrangian density is[1]

$$\begin{aligned}\mathcal{L}=&\bar{\psi}[\gamma_\mu(i\partial^\mu-g_v V^\mu)-(M-g_s\phi)]\psi \\ &+\tfrac{1}{2}(\partial_\mu\phi\partial^\mu\phi-m_s^2\phi^2)-\tfrac{1}{4}(\partial_\mu V_\nu-\partial_\nu V_\mu)^2 \\ &+\tfrac{1}{2}m_v^2 V_\mu V^\mu-V(\phi)+\delta\mathcal{L}\ , \end{aligned} \tag{2.1}$$

where

$$V(\phi)=\frac{\kappa}{3!}\phi^3+\frac{\lambda}{4!}\phi^4$$

and $\delta\mathcal{L}$ is a counterterm Lagrangian. For phenomenological purposes, we allow λ to be negative, even though this leads to a classical potential unbounded from below; the rationale for permitting negative λ is discussed in Sec. IV and in Ref. 10. In cases of interest, the energy functional has a well-defined minimum, which is nonetheless only a local minimum. We note that, even in the absence of $V(\phi)$, the one-loop (RHA) effective potential is unbounded from below.

We consider the mean-field (Hartree) approximation to this theory, in which the meson field operators are replaced by their expectation values, which are classical fields. (Alternatively, it follows from the self-consistent sum of tadpole contributions to the baryon propagator.[3]) This approximation is often motivated as a high-density limit of the field theory; at normal nuclear densities, the mean-field theory provides a nonperturbative starting point for describing the nuclear many-body system. Mean-field models have had many phenomenological successes, but it is still not clear whether the simple physical picture described by the mean-field theory (or the RHA) is an accurate representation of the underlying quantum field theory. Corrections to the self-consistent Hartree approximation (e.g., Hartree-Fock) can be investigated systematically in quantum hadrodynamics.

To realistically describe finite nuclei, the σ-ω model is extended to include rho mesons, pions, and photons. We follow Ref. 3 to derive the mean-field equations, extending the results obtained there by relaxing the assumption of spherical symmetry. The nuclear ground state is still assumed to have good parity and well-defined charge. Initially, we neglect contributions from the negative-energy Dirac sea; the extension to the relativistic Hartree approximation (RHA) is discussed below.

The equations for the neutral meson fields are

$$\begin{aligned}(\nabla^2-m_s^2)\phi(\mathbf{x})&=-g_s\sum_\alpha^{\text{occ}}\bar{U}_\alpha(\mathbf{x})U_\alpha(\mathbf{x}) \\ &\quad+\frac{\kappa}{2}\phi^2+\frac{\lambda}{6}\phi^3 \\ &\equiv -g_s[\rho_s(\mathbf{x})+\Delta\rho_s(\mathbf{x})]\ , \end{aligned} \tag{2.2}$$

$$(\nabla^2-m_v^2)V_0(\mathbf{x})=-g_v\sum_\alpha^{\text{occ}} U_\alpha^\dagger(\mathbf{x})U_\alpha(\mathbf{x})$$
$$\equiv -g_v\rho_B(\mathbf{x}) , \tag{2.3}$$

and

$$(\nabla^2-m_v^2)\mathbf{V}(\mathbf{x})=-g_v\sum_\alpha^{\text{occ}} U_\alpha^\dagger(\mathbf{x})\boldsymbol{\alpha}U_\alpha(\mathbf{x})$$
$$\equiv -g_v\mathbf{J}_B(\mathbf{x}) , \tag{2.4}$$

where the sums run over occupied positive-energy states, and we have defined the contributions from the scalar self-couplings in Eq. (2.2) to be $-g_s\Delta\rho_s$ ($\boldsymbol{\alpha}$ is the usual Dirac matrix.) There are equations analogous to (2.3) and (2.4) for the other vector mesons, with appropriate isospin factors. Each single-particle spinor $U_\alpha(\mathbf{x})$ satisfies a Dirac equation

$$hU_\alpha(\mathbf{x})=\epsilon_\alpha U_\alpha(\mathbf{x}) , \tag{2.5}$$

where the single-particle Dirac Hamiltonian h is

$$h\equiv\{\boldsymbol{\alpha}\cdot[-i\nabla-g_v\mathbf{V}(\mathbf{x})]+\beta[M-g_s\phi_0(\mathbf{x})]$$
$$+g_vV_0(\mathbf{x})\} , \tag{2.6}$$

and where we have suppressed the contributions from the rho and photon fields. Equations (2.2)–(2.6) are nonlinear, coupled partial differential equations, which must be solved self-consistently.

For closed-shell nuclei, the equations are greatly simplified by the assumption of spherical symmetry. In this case, the three-vector field $\mathbf{V}$ and the baryon current $\mathbf{J}_B$ vanish and the other meson fields depend only on $|\mathbf{x}|$. Recent calculations have relaxed this assumption, and the Hartree equations for deformed even-even nuclei have been solved assuming only axial symmetry.[7–11] (A triaxial calculation is discussed in Ref. 30.) In these calculations, single-nucleon levels are no longer eigenstates of total angular momentum j, but j_z and parity are still good quantum numbers. Nucleons are paired in degenerate $j_z=\pm m$ states so that the three-vector field and the baryon current still vanish. In Refs. 9 and 10, on which we base the present work, the angular dependence of the remaining fields and sources are expanded in even Legendre polynomials and the nucleon wave functions are expanded in spherical basis functions, resulting in coupled, ordinary differential equations that are solved iteratively.[9]

The further extension to odd-A nuclei near closed shells is straightforward if we make certain assumptions about the self-consistent ground state. Take as the starting point the extreme shell-model picture of a spherical core (solved self-consistently) to which a valence particle or hole is added in a definite m state. The system is no longer self-consistent because of the new meson fields generated by the valence particle, which include a three-vector field. These additional fields modify the single-particle Hamiltonian h so that the core wave functions are altered. These changes are the source of new meson fields that modify all of the wave functions further, and so on, until self-consistency is restored.

The self-consistent solution will be a deformed intrinsic state without definite total angular momentum. However, the nucleon orbitals will still have good j_z and parity. The degeneracy of $+m$ and $-m$ states will be broken (they will no longer appear in time-reversed pairs), but otherwise the equations are very similar to those already solved for deformed even-even nuclei. The only new addition is $\mathbf{V}(\mathbf{x})$ and its form is simplified by the surviving symmetries. In particular, if this field is expanded in vector spherical harmonics, $\mathbf{Y}_{JL1}^{M}$,[31] only the $\mathbf{Y}_{LL1}^{M=0}$ terms with odd L will be nonzero. Thus the generalization from even-even nuclei involves only one additional radial function for each L [the $V^L(r)$ in Eq. (2.9)]. We also note that an extended model will have a nonvanishing pion field.

Equation (2.4) gives the convection (baryon) current $\mathbf{J}_B(\mathbf{x})$ directly as a sum over contributions from the occupied states and the Dirac equation can be used to show that this current is divergenceless ($\nabla\cdot\mathbf{J}_B=0$). This expression for the current is simple because it is written in terms of the self-consistent basis. Contributions from the core states can be compared with the core response calculated in linear response (RPA) treatments given elsewhere.[26–28] The contribution from the valence nucleon will still exhibit the familiar M/M^* enhancement, but we expect that nonzero contributions from the core will cancel the enhancement at low q, as found in nuclear matter.[24]

The mean-field equations for deformed nuclei have been solved using several different methods.[7–9] Here we follow Ref. 9 and expand each of the mean fields and the source densities in an angular basis. As noted above, the assumed nuclear symmetries significantly restrict the expansions. The scalar field and the time components of the vector fields are expanded in (even) Legendre polynomials. For example,

$$\phi(\mathbf{x})=\sum_{L\ \text{even}}^{L_{\max}}\phi^L(r)P_L(\cos\theta) , \tag{2.7}$$

$$V_0(\mathbf{x})=\sum_{L\ \text{even}}^{L_{\max}}V_0^L(r)P_L(\cos\theta) . \tag{2.8}$$

The three-vector fields are expanded in vector spherical harmonics; only the $\mathbf{Y}_{LL1}^{M=0}$ terms are needed and only odd L contribute, so the three-vector field is purely azimuthal:

$$\mathbf{V}(\mathbf{x})=\sum_{L\ \text{odd}}^{L_{\max}} iV^L(r)\mathbf{Y}_{LL1}^{M=0*}(\Omega_x)$$
$$=\hat{\varphi}\sum_{L\ \text{odd}}^{L_{\max}}V^L(r)\left[\frac{2L+1}{4\pi L(L+1)}\right]^{1/2}P_L^1(\cos\theta) , \tag{2.9}$$

where P_L^1 is an associated Legendre polynomial. We truncate the expansions at $L=L_{\max}$.

The nucleon orbitals are expanded in terms of spherical spin-angle functions:

$$U_\alpha(\mathbf{x}) \equiv U_{\alpha mt}(\mathbf{x}) = \sum_{\kappa'} \begin{bmatrix} \dfrac{iG^\alpha_{\kappa' mt}(r)}{r}\Phi_{\kappa' m} \\ \dfrac{-F^\alpha_{\kappa' mt}(r)}{r}\Phi_{-\kappa' m} \end{bmatrix} \eta_t \ , \tag{2.10}$$

where η_t is an isospinor and κ' is the usual relativistic angular quantum number.[1] The allowed values of κ' are limited by the symmetries and $L_{\max}$. In particular, only terms with the same parity are included in the sum. For nuclei near closed shells, the sum for a particular occupied level is dominated by the term that would survive in the spherical limit (no core deformation). We designate the quantum numbers of this term by $\kappa_{\rm sph}$ and $j_{\rm sph}$. Then the sum in (2.10) includes all κ' (and corresponding j') such that

$$|j_{\rm sph} - L_{\max}| \le j' \le j_{\rm sph} + L_{\max} \ . \tag{2.11}$$

Note that the total angular momentum j of an individual orbital is no longer a good quantum number but m is still good. If we perform calculations with $L_{\max}=0$, the wave functions do not mix, the core does not deform, and the spherical-limit quantum numbers are restored.

If the expansions (2.7)–(2.10) are substituted into (2.2)–(2.5), equations with different L's decouple and the problem is reduced to a system of coupled ordinary differential equations. These equations are solved by an iterative procedure similar to that described in Ref. 9. The only new feature is the addition of $\Delta\rho_s$ to the scalar field equation. This new term is expanded in Legendre polynomials numerically and, since $\Delta\rho_s$ depends on ϕ, Eq. (2.2) is solved iteratively. More details on the solution method are given in the Appendix.

B. Elastic magnetic scattering

We will use elastic magnetic scattering of electrons from nuclei, which probes ground-state nuclear currents, to compare Hartree predictions to experiment. Following the discussion in Ref. 32, we introduce an effective electromagnetic current operator

$$\hat{J}^\mu(x) \doteq \bar{\psi}(x)\gamma^\mu Q\psi(x) + \frac{1}{2M}\partial_\nu[\bar{\psi}(x)\lambda\sigma^{\mu\nu}\psi(x)] \ , \tag{2.12}$$

where the field operators are in the Heisenberg representation, and

$$\begin{aligned} Q &\equiv \tfrac{1}{2}(1+\tau_3) \ , \\ \lambda &\equiv \lambda_p \tfrac{1}{2}(1+\tau_3) + \lambda_n \tfrac{1}{2}(1-\tau_3) \ , \end{aligned} \tag{2.13}$$

are the charge and anomalous magnetic moment operators.

The transverse elastic form factor for a nuclear state $|J_i\rangle$ is given by[33]

$$F_T^2(q) = \frac{f_{sn}^2(q) f_{\rm c.m.}^2(q)}{2J_i+1} \sum_{J=1,3,\ldots}^{2J_i} |\langle J_i \| \hat{T}^{\rm mag}_J(q) \| J_i \rangle|^2 \ , \tag{2.14}$$

where q denotes the magnitude of the three-momentum transfer. The transverse magnetic multipole operators are defined in terms of the Schrödinger picture nuclear current density operator $\hat{J}^\mu(\mathbf{x})$ by

$$\hat{T}^{\rm mag}_{JM}(q) \equiv \int d^3x \, j_J(qx) \mathbf{Y}^M_{JJ1}(\Omega) \cdot \hat{\mathbf{J}}(\mathbf{x}) \ , \tag{2.15}$$

where j_J is a spherical Bessel function, $\mathbf{Y}^M_{JJ1}$ is a standard vector spherical harmonic,[31] and $\hat{J}^\mu(\mathbf{x}) \equiv [\hat{\rho}(\mathbf{x}), \hat{\mathbf{J}}(\mathbf{x})]$. Once elastic magnetic form factors have been computed, the ground-state magnetic dipole moment μ follows from the $q \to 0$ limit

$$\mu = \lim_{q\to 0} \left\{ -i \left[\frac{2M}{q} \right] \left[\frac{6\pi J_i}{(J_i+1)(2J_i+1)} \right]^{1/2} \times \langle J_i \| \hat{T}^{\rm mag}_{J=1}(q) \| J_i \rangle \right\} . \tag{2.16}$$

Only the $M1$ multipole contributes to the magnetic moment.

For elastic transitions, the three-vector current operator in the Schrödinger picture reduces to

$$\hat{\mathbf{J}}(\mathbf{x}) = \psi^\dagger(\mathbf{x}) Q\boldsymbol{\alpha}\psi(\mathbf{x}) + \frac{1}{2M}\nabla \times [\psi^\dagger(\mathbf{x})\lambda\beta\boldsymbol{\Sigma}\psi(\mathbf{x})] \ . \tag{2.17}$$

Here $\boldsymbol{\alpha}$ and β are the usual Dirac matrices and

$$\boldsymbol{\Sigma} = \begin{bmatrix} \boldsymbol{\sigma} & 0 \\ 0 & \boldsymbol{\sigma} \end{bmatrix} .$$

In the Hartree approximation to the nuclear ground state, the elastic matrix element of this current is given by

$$\langle J_i | \hat{\mathbf{J}}(\mathbf{x}) | J_i \rangle = \sum_\alpha^{\rm occ} U^\dagger_\alpha(\mathbf{x}) Q\boldsymbol{\alpha} U_\alpha(\mathbf{x}) + \frac{1}{2M}\nabla \times \sum_\alpha^{\rm occ} U^\dagger_\alpha(\mathbf{x})\lambda\beta\boldsymbol{\Sigma} U_\alpha(\mathbf{x}) \ , \tag{2.18}$$

where the $U_\alpha(\mathbf{x})$ are the self-consistent (positive-energy) single-particle solutions for the finite nucleus. Thus, the calculation of nuclear matrix elements reduces to a sum of single-particle matrix elements. [The first term in (2.18) is the Dirac convection current and the second term is the anomalous current.] Expressions for matrix elements of the corresponding single-particle operator $\hat{T}^{\rm mag}_J$ are given in the Appendix. Additional details on calculating the form factors (single-nucleon form factors, center-of-mass correction, etc.) can be found in Refs. 1 and 32.

In some RPA discussions (e.g., Ref. 28), core-polarization effects are discussed as a modification of the vertex for the valence nucleon (i.e., a renormalization of the nucleon form factor). We emphasize that by using *self-consistent* Hartree wave functions in Eq. (2.18), we incorporate the same physics.[24] In a full self-consistent

RHA calculation, the renormalization due to the Dirac sea appears as the contribution to the current from the deformed Dirac sea, which can be calculated in a finite nucleus in a derivative expansion, as in (2.23). A complete and consistent treatment of the single-nucleon form factors is beyond the scope of the Hartree approximation, which does not have contributions from charged mesons. Note, however, that when (isoscalar) vacuum polarization is included (i.e., the RHA), the experimental form factor should be adjusted for the screening at zero density by the Dirac sea. This issue will be addressed in a forthcoming paper, which includes RHA derivative corrections.

As indicated by the notation, we assume that the ground states are approximately eigenstates of total **J**, despite the deformation. Because we do not project states of good J, we restrict ourselves to elastic magnetic scattering from nuclei near closed shells that do not exhibit large core deformations. The approximation can be checked by computing the ratio of currents obtained when the valence nucleon is placed in different m states.

C. Relativistic Hartree approximation

The equations given earlier are easily modified to include nucleon one-loop contributions; this approximation is conventionally called the relativistic Hartree approximation. Originally, the vacuum corrections in the RHA for finite spherical nuclei were included only in a local density approximation.[1] Perry[34] and Wasson[35] have recently considered derivative corrections to the nuclear matter results, which are nonnegligible in finite nuclei. In particular, we expect that the correction to the baryon current from the deformed Dirac sea will be significant. However, in the present work we will only give results for corrections included in the local density approximation.

To extend Eqs. (2.2)–(2.6) to the RHA, the only changes are additional densities $g_s\Delta\rho_s^{\rm vac}(\mathbf{x})$, $g_v\Delta\rho_B^{\rm vac}(\mathbf{x})$, and $g_v\Delta\mathbf{J}_B^{\rm vac}(\mathbf{x})$, which are added to the right-hand sides of the meson equations (2.2)–(2.4), respectively. If we include the leading derivative corrections, these are given explicitly by

$$\Delta\rho_s^{\rm vac}(\mathbf{x})=-\frac{1}{\pi^2}\left[M^{*3}\ln\left[\frac{M^*}{M}\right]+\tfrac{1}{3}M^3-\tfrac{3}{2}M^2M^*+3MM^{*2}-\tfrac{11}{6}M^{*3}\right]$$
$$-\frac{1}{4\pi^2}\left[2\ln\left[\frac{M^*}{M}\right]\nabla^2(g_s\phi)-\frac{1}{M^*}(\nabla g_s\phi)^2\right]-\frac{1}{12\pi^2}\frac{1}{M^*}g_v^2F_{\mu\nu}F^{\mu\nu}\ , \tag{2.19}$$

$$(\Delta\mathbf{J}_B^{\rm vac})^\mu(\mathbf{x})=\frac{1}{3\pi^2}\partial_\nu\left[\ln\left[\frac{M^*}{M}\right]g_vF^{\nu\mu}\right]\ , \tag{2.20}$$

where

$$(\Delta\mathbf{J}_B^{\rm vac})^\mu(\mathbf{x})\equiv[\Delta\rho_B^{\rm vac}(\mathbf{x}),\Delta\mathbf{J}_B^{\rm vac}(\mathbf{x})]\ .$$

The meson fields and $M^*\equiv M-g_s\phi$ are functions of $\mathbf{x}$, and $F_{\mu\nu}\equiv\partial_\mu V_\nu-\partial_\nu V_\mu$ can be simplified since $V_\mu(\mathbf{x})$ is independent of time. For the meson fields of Eqs. (2.7)–(2.9), these expressions reduce to

$$\Delta\rho_s^{\rm vac}(\mathbf{x})=-\frac{1}{\pi^2}\left[M^{*3}\ln\left[\frac{M^*}{M}\right]+\tfrac{1}{3}M^3-\tfrac{3}{2}M^2M^*+3MM^{*2}-\tfrac{11}{6}M^{*3}\right]$$
$$-\frac{1}{4\pi^2}\left[2\ln\left[\frac{M^*}{M}\right]\nabla^2(g_s\phi)-\frac{1}{M^*}(\nabla g_s\phi)^2\right]+\frac{1}{6\pi^2}\frac{1}{M^*}[(\nabla g_vV_0)^2-(\nabla g_vV_\varphi\hat{\varphi})^2]\ , \tag{2.21}$$

$$\Delta\rho_B^{\rm vac}(\mathbf{x})=-\frac{1}{3\pi^2}\nabla\cdot\left[\ln\left[\frac{M^*}{M}\right]\nabla g_vV_0\right]\ , \tag{2.22}$$

$$\Delta\mathbf{J}_B^{\rm vac}(\mathbf{x})=-\frac{1}{3\pi^2}\nabla\cdot\left[\ln\left[\frac{M^*}{M}\right]\nabla g_vV_\varphi\hat{\varphi}\right]\ , \tag{2.23}$$

where the fields are functions of r and θ only and we have defined V_φ through $\mathbf{V}(\mathbf{x})\equiv V_\varphi(r,\theta)\hat{\varphi}$. (Note that $\nabla\hat{\varphi}\neq0$.) In spherical nuclei, for which $V_\varphi=0$, Eqs. (2.21) and (2.22) agree with those used by Wasson.[34]

In the local density approximation used in this paper, all derivative terms are neglected, leaving only the first term in brackets in Eq. (2.21). [In particular, the vacuum current (2.23) is not included.] The derivative corrections will be included in a forthcoming investigation.

III. RESULTS

In this section, we present results from self-consistent Hartree calculations of odd-A nuclei. First, we consider the bulk systematics of light nuclei (binding energies, rms radii, and quadrupole moments), and then turn to magnetic moments and currents. Angular momentum projection is not included; all results are for intrinsic states. Since we are considering nonspherical nuclei, the

ground-state solutions are mixtures of states with different total angular momentum, and the true ground state should be obtained from the intrinsic solution by projection. Instead, we relate quadrupole moments to experiment by assuming the nonrelativistic collective model is applicable. Magnetic moments and currents are discussed only for nuclei near closed shells, with small core deformations. A measure of the importance of the deformations is obtained by considering the relative sizes of the various components of Eq. (2.10). As long as each nuclear orbital is predominately made up of a single component in the expansion, the intrinsic ground state should be an approximate eigenstate of the total angular momentum. Except when noted explicitly, we do not believe that the lack of angular momentum projection affects our discussion.

All results reported here were generated using two independent codes that used the expansion techniques described in Sec. II and the Appendix. For odd-A nuclei, the expansions were truncated at $L_{\max}=3$, with selected runs at $L_{\max}=4$ to check convergence. (Even-even nuclei in Figs. 1–4 were calculated with $L_{\max}=4$.) This provides adequate convergence for the observables presented here. The significant figures given in the tables reflect the numerical precision of the calculations.

We start by examining the systematics of bulk properties of nuclei, including results for even-even nuclei discussed in more detail in Ref. 10. In that work, a wide variety of mean-field parameter sets were considered, with each adjusted to reproduce "empirical" nuclear matter saturation properties, taken to be a binding energy of 15.75 MeV at an equilibrium density corresponding to $k_F=1.3$ fm^{-1}, and the rms charge radius of ^{40}Ca. For the present survey, we have selected three sets, as given in Table I. The linear set (L) is essentially the same as the standard parametrization of Horowitz and Serot,[3] while the nonlinear set (NL) is similar to the set obtained in Ref. 5, as providing the best fit to properties of spherical nuclei.[36] Later, we consider a one-loop (RHA) model, using parameters very similar to those given in Ref. 1.

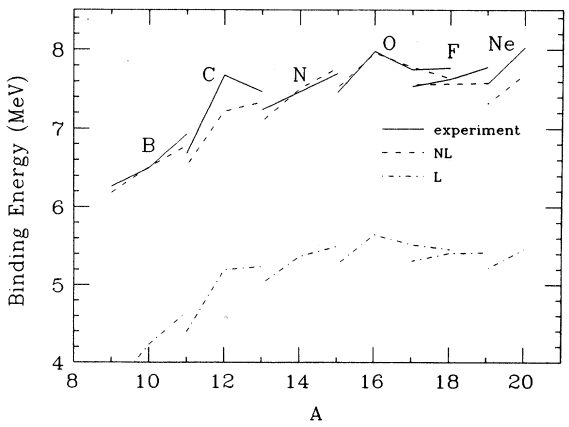

FIG. 1. Binding energy per nucleon of light nuclei for the linear (dot-dashed) and nonlinear (dashed) parameter sets from Table I, compared with experimental data (solid).

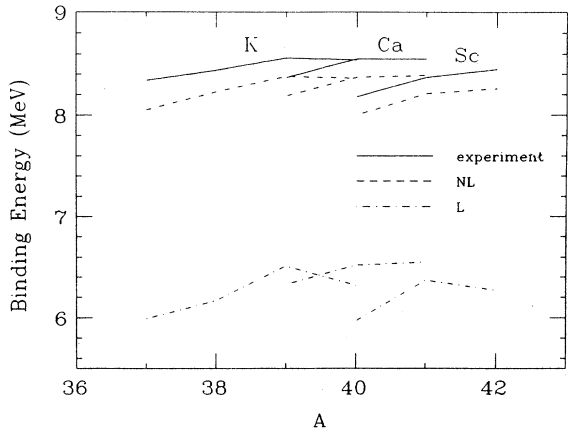

FIG. 2. Binding energy per nucleon of nuclei near ^{40}Ca for the linear (dot-dashed) and nonlinear (dashed) parameter sets from Table I, compared with experimental data (solid).

Binding energies per nucleon of nuclei from boron to neon are plotted in Fig. 1 for the linear and nonlinear parameter sets, and compared to experiment. Figure 2 shows results for nuclei near ^{40}Ca. The binding energies include a correction for the center-of-mass energy as in Ref. 5, but no correction for angular momentum projection, which would tend to increase binding somewhat. Binding-energy systematics are well reproduced by the mean-field calculations using the nonlinear parameter set, including the pattern of even and odd nuclei with the same Z. The self-consistent ground states exhibit a preference for pairs of approximately time-reversed states to be filled, despite the explicit lack of pairing; similar results have been noted in nonrelativistic Hartree-Fock calculations.[37,38]

The linear and nonlinear models show similar trends, but the linear nuclei are systematically underbound. As

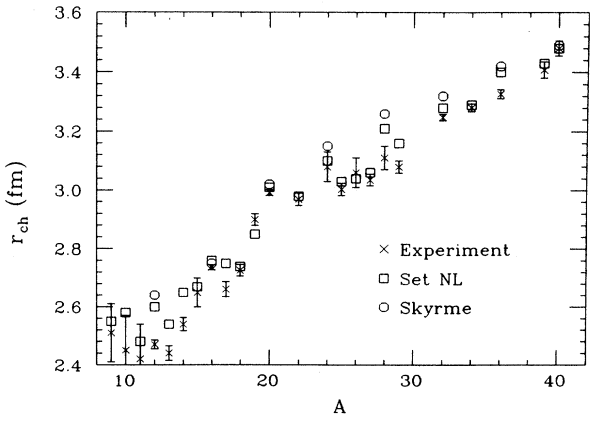

FIG. 3. Rms charge radii of s-d shell nuclei for the nonlinear (□) parameter set from Table I and a nonrelativistic Hartree-Fock calculation with the Skyrme II interaction (○) from Ref. 39, compared with experimental data (×) from Ref. 40.

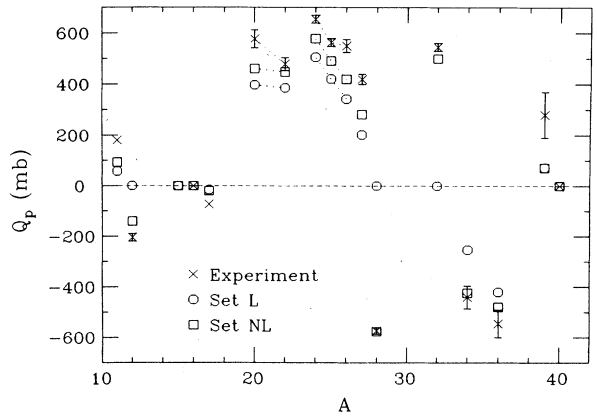

FIG. 4. Intrinsic charge quadrupole moments (mb) of *s-d* nuclei for the linear (○) and nonlinear (□) parameter sets from Table I. Moments derived from experimental measurements (×) are taken from Refs. 42 and 43.

shown in Ref. 10, this is directly attributable to the large surface energy that is characteristic of linear mean-field models. We note that only parameter sets with negative values of λ [see Eq. (2.1)] have sufficiently reduced surface energies to quantitatively reproduce experimental binding energies.

Calculated rms charge radii from boron to calcium are plotted in Fig. 3 for the nonlinear parameter set, and compared to experiment. To compare to nonrelativistic models, rms radii for the Skyrme interaction from Ref. 39 are also included. Predictions for the radii are reasonable, and generally similar to the Skyrme predictions. Once again, the radii are for intrinsic states; projection should improve the agreement for light nuclei.

Intrinsic quadrupole moments for selected nuclei in the *s-d* shell are shown in Fig. 4. We compare to "experimental" intrinsic quadrupole moments that are extracted from $B(E2)$ data (even-even nuclei) or spectroscopic data (odd-A nuclei) using model-dependent assumptions. (For example, a rotational model is assumed. See Refs. 40 and 41 for details on the assumptions made in extracting intrinsic moments.) Because of the approximations involved, quantitative comparisons to experiment must be viewed with some caution, so we focus on systematic trends.

As noted in Ref. 10, the systematics of even-even nuclei are well reproduced by the nonlinear set, including the pattern of oblate and prolate deformations. This success continues for odd-A nuclei (for which data are available). In addition, the systematics are similar to those found in nonrelativistic Hartree-Fock calculations, although for ^{27}Al the relativistic calculation predicts the opposite (and experimentally correct) deformation.[37] The linear model predicts smaller deformations in general and no deformations for closed subshell nuclei. This difference between the models is closely related to the strength of the spin-orbit splitting, which is somewhat too large in the linear model.[10]

Next we turn to magnetic moments, starting with isoscalar moments for $N=Z$ nuclei. Table II shows isoscalar moments from the self-consistent calculations, using the three models from Table I. The column labeled "Orbital" gives the quantum numbers of the dominant component of the valence wave function. The moments in the "valence" column are calculated using $L_{\max}=0$ in the angular expansions (see Sec. II). In this case, the core wave functions do not mix and the moment is entirely due to the valence contribution. As a result, the moments reflect the M/M^* enhancement of the valence current that is the source of the "magnetic moment problem." (The valence moments are given for the linear model; moments for the nonlinear model of the RHA would be somewhat less enhanced because M^*/M is close to one.)

The self-consistent moments show a remarkable consistency and all are close to the Schmidt values. Thus, isoscalar moments are not only insensitive to relativistic effects, they are insensitive to details of the models. Experimental moments are also close to the Schmidt values. We note that corrections to nonrelativistic Schmidt predictions, which have been studied extensively,[41] should also be relevant in the relativistic calculations.

In Table III, self-consistent isoscalar moments for linear and nonlinear models are compared to moments obtained using linear response theory (RPA).[27] In this case, the linear parameters are from Ref. 3, the nonlinear parameters are from Ref. 5, and the rho and Coulomb interactions are turned off. Moments predicted by the two methods are essentially equivalent, showing that the isoscalar moments are not sensitive to the differences between the approximations.

Further insight into the nature of the core response to the valence nucleon (particle or hole) can be found from Table IV, where individual contributions from single-nucleon states to the isoscalar Dirac moment in an $A=39$ nucleus are given. Results for $L_{\max}=0$ (no wave-function mixing) are compared to $L_{\max}=3$ (maximal mixing of wave functions). The levels are labeled by the quantum numbers of the $L_{\max}=0$ calculations; the dominant components of the mixed wave functions when

TABLE I. Parameters for mean-field models used in the self-consistent calculations. Linear (L), nonlinear (NL), and one-loop (RHA) sets are from Ref. 10.

Model	g_s^2	g_v^2	g_ρ^2	m_s	κ	λ	M^*/M
L	109.73	190.59	65.37	520.1	0	0	0.54
NL	95.11	148.93	74.99	500.8	5000	−200	0.63
RHA	54.04	102.58	83.30	457.3	0	0	0.73

TABLE II. Isoscalar magnetic moments using linear, nonlinear, and RHA self-consistent models (see Table I) for $N=Z$ nuclei. Valence only moments are for the linear model.

A	Orbital	Schmidt	Valence	L	NL	RHA	Expt.
11	$1p\frac{3}{2}$	0.940	1.13	0.96	0.96	0.96	0.892
13	$1p\frac{1}{2}$	0.187	0.307	0.182	0.180	0.172	0.190
15	$1p\frac{1}{2}$	0.187	0.343	0.199	0.195	0.191	0.218
17	$1d\frac{5}{2}$	1.440	1.57	1.43	1.44	1.44	1.414
39	$1d\frac{3}{2}$	0.636	1.01	0.66	0.66	0.65	0.706
41	$1f\frac{7}{2}$	1.940	2.26	1.94	1.94	1.95	1.918

$L_{\max}=3$ retain these quantum numbers. Contributions from levels that are exact time-reversed pairs in the $L_{\max}=0$ case are grouped together.

When no core polarization is allowed ($L_{\max}=0$), contributions to the current from time-reversed states cancel exactly, leaving the contribution from the valence nucleon (a hole in this case) uncanceled and providing the entire moment. When the core wave functions are allowed to mix, the valence moment is essentially unchanged, but the states that previously canceled are no longer exact time-reversed pairs and the cancellation of Dirac moment contributions is incomplete. The net contribution from each pair adds *coherently* to the isoscalar moment, as predicted from nuclear matter results.[24] The final result is that the "core response" restores the predicted Dirac moment to the Schmidt value. RPA calculations of finite nuclei in Ref. 27 showed that, in terms of the spherical basis states, it is the mixing of negative-energy wave functions into the spherical core wave functions that is responsible for these contributions to the moment. The three-vector field **V** is also clearly essential for these contributions, since it breaks the time-reversal symmetry of the core states. The entire effect is mediated by this field in the linear response calculations.

In Figs. 5 and 6, the isoscalar $J=1$ convection (Dirac) current is shown for $A=15$, in coordinate space and momentum space, respectively. [The definitions of the functions $b_J(r)$ and $\tilde{b}_J(q)$ are given in the Appendix.] The dot-dashed curve is the contribution from the valence wave function only ($L_{\max}=0$), and it can be compared to the dotted curve, labeled "nonrelativistic." The latter curve is obtained from the valence Dirac spinor by fixing the upper component and generating a new lower component using the free-space Dirac equation (with $M^*=M$). This curve *simulates* the Dirac convection current due to a nonrelativistic wave function for the valence nucleon, and serves to quantify M^* effects. The M/M^* enhancement of the valence current is apparent in both coordinate and momentum space.

The solid and dashed curves are from self-consistent and RPA calculations of the current, respectively. Evidently, these approximations predict similar currents, in both coordinate and momentum space. The small differences between the curves primarily reflect differences in the contributions of the valence nucleon. In the linear response calculation, the valence wave function is unchanged and is determined by the meson fields of the core alone, while in the self-consistent calculation it participates fully in the mixing of wave functions.

In momentum space, the self-consistent current (and RPA current) is close to the "nonrelativistic" curve at low q and is suppressed relative to the valence current. This is consistent with the magnetic moment results of Table II, since the slope of $\tilde{b}_J(q)$ at low q is proportional to the magnetic moment. At higher q, the self-consistent current is enhanced; this effect is universal in mean-field models (but not RHA models) and is consistent with the nuclear matter response predicted by these models.[27]

Isoscalar contributions to the anomalous current in momentum space are shown in Fig. 7. The dominant feature here is the enhancement of the self-consistent current relative to the valence current from an $L_{\max}=0$ calculation. Such differences have little effect on predictions for isoscalar moments, because of the small isoscalar anomalous moment of the nucleon. However, much of the difference comes from changes in the valence wave function, as opposed to the core response, which can have important effects on predictions for isovector moments and elastic magnetic form factors. In addition, the amount of wave-function mixing can depend strongly on $L_{\max}$, particularly for $J>1$.

In general, isovector moments and currents are far

TABLE III. Isoscalar moments for linear (L') and nonlinear (NL') models calculated using different approximations: valence only, RPA, and self-consistent. The calculations were performed using parameter sets from Refs. 3 and 5.

	$A=15$		$A=17$		$A=39$		$A=41$	
	L'	NL'	L'	NL'	L'	NL'	L'	NL'
Valence only	0.350	0.321	1.57	1.56	1.03	0.96	2.28	2.22
RPA	0.204	0.202	1.44	1.44	0.66	0.66	1.95	1.95
Self-consistent	0.195	0.195	1.45	1.44	0.66	0.66	1.96	1.94

TABLE IV. Contributions to the isoscalar Dirac magnetic moment from single-particle levels in an $A=39$ nucleus, using the linear parameter set from Ref. 3, as in Table III. Calculations with $L_{max}=0$ and 3 are compared.

		μ_D, $L_{max}=0$			μ_D, $L_{max}=3$		
Level	$\|m\|$	$+\|m\|$	$-\|m\|$	Net	$+\|m\|$	$-\|m\|$	Net
$1s\frac{1}{2}$	$\frac{1}{2}$	+1.58	−1.58	0.0	+1.55	−1.61	−0.06
$1p\frac{3}{2}$	$\frac{1}{2}$	+0.94	−0.94	0.0	+0.96	−1.10	−0.04
$1p\frac{3}{2}$	$\frac{3}{2}$	+2.83	−2.83	0.0	+2.80	−2.85	−0.05
$1p\frac{1}{2}$	$\frac{1}{2}$	+0.80	−0.80	0.0	+0.73	−0.79	−0.06
$1d\frac{5}{2}$	$\frac{1}{2}$	+0.77	−0.77	0.0	+0.76	−0.80	−0.04
$1d\frac{5}{2}$	$\frac{3}{2}$	+2.30	−2.30	0.0	+2.30	−2.34	−0.04
$1d\frac{5}{2}$	$\frac{5}{2}$	+3.83	−3.83	0.0	+3.82	−3.84	−0.02
$2s\frac{1}{2}$	$\frac{1}{2}$	+1.14	−1.14	0.0	+1.16	−1.18	−0.02
$1d\frac{3}{2}$	$\frac{1}{2}$	+0.66	−0.66	0.0	+0.61	−0.62	−0.01
$1d\frac{3}{2}$	$\frac{3}{2}$	+1.97	−1.97	0.0	+1.94	−1.96	−0.02
Core				0.0			−0.36
Valence	$\frac{3}{2}$			+0.99			+0.97
Total				+0.99			+0.61

more sensitive to details of the model and the approximation used. Magnetic moments for a range of nuclei near closed shells are given in Table V for the linear and nonlinear models of Table I. Given the uniform predictions for isoscalar moments cited above, the discrepancies between predictions reflect differences in the isovector moments. Table VI includes a decomposition of the moments for the heavier nuclei into Dirac and anomalous moments for $L_{max}=0$ and 3 linear model calculations, indicating core and valence contributions separately. As seen for the light nuclei, core polarization plays an important role in determining the Dirac moment. The anomalous moments are strongly affected by core deformations, both through the contribution of the valence state and the direct contributions from the core. The nuclei with valence holes in Table VI are particularly susceptible to wave-function mixing because the valence nucleon starts out as a $p\frac{1}{2}$ state. Because of other well-known many-body and exchange-current contributions to isovector magnetic moments, comparisons to experiment are not very meaningful at this point. We simply present the results and note that further study of the isovector moments, including contributions from pions, is needed.

Finally, we consider elastic magnetic scattering as a probe of ground-state currents at finite q. Transverse magnetic form factors are shown for ^{15}N in Figs. 8 and 9, for ^{17}O in Fig. 10, and for ^{209}Bi in Figs. 11 and 12. Curves labeled "valence only" are from self-consistent

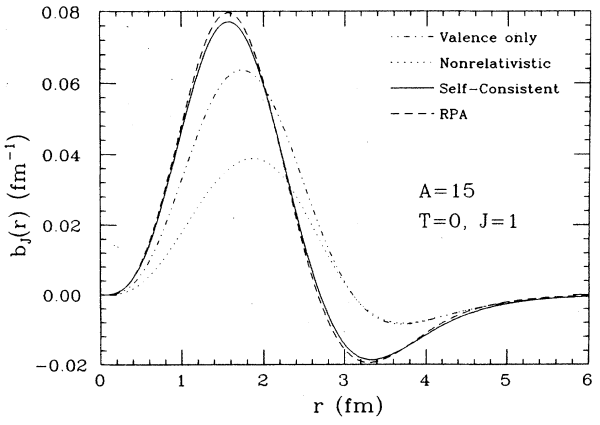

FIG. 5. The isoscalar, $J=1$ convection current for $A=15$, in coordinate space, calculated for the linear model with no Coulomb interaction. The curves are valence only (dot-dashed), nonrelativistic (dotted), fully self-consistent (solid), and RPA (dashed).

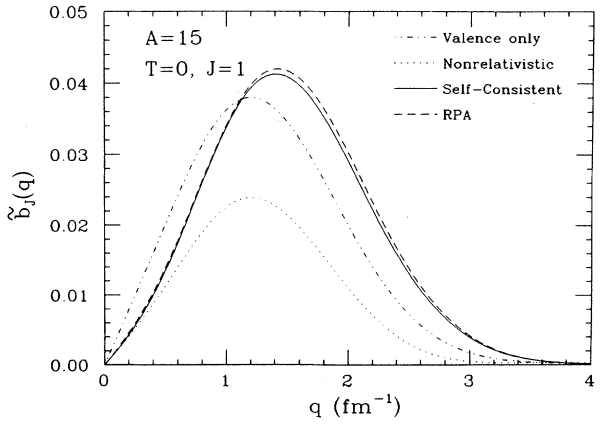

FIG. 6. The isoscalar, $J=1$ convection current for $A=15$, in momentum space, calculated for the linear model with no Coulomb interaction. The curves are valence only (dot-dashed), nonrelativistic (dotted), fully self-consistent (solid), and RPA (dashed).

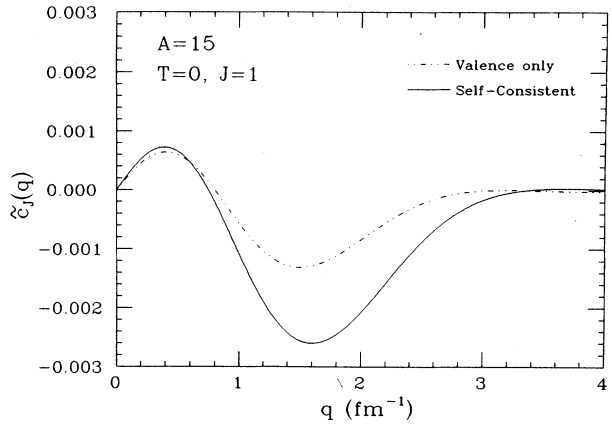

FIG. 7. The isoscalar, $J=1$ anomalous current for $A=15$, in momentum space, calculated for the linear model with no Coulomb interaction. The curves are valence only (dot-dashed) and fully self-consistent (solid).

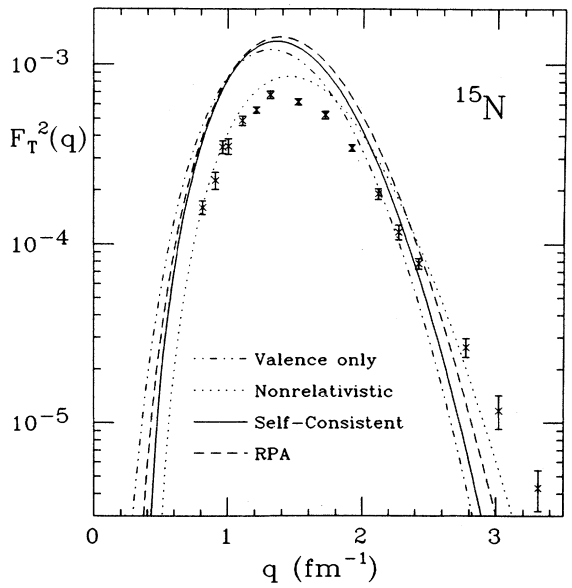

FIG. 8. Elastic magnetic form factor for ^{15}N, using the linear model parameters. The dot-dashed curve is valence only, the dotted curve is a Schrödinger-equivalent calculation, the solid curve is the self-consistent Hartree calculation, and the dashed curve is an RPA calculation from Ref. 27. Experimental data are from Ref. 44.

$L_{\max}=0$ calculations and those labeled nonrelativistic are calculated from Schrödinger-equivalent valence wave functions.[1]

The valence only (impulse approximation) curve for ^{15}N shows a large enhancement of the isoscalar current relative to the Schrödinger-equivalent curve. Because the wave function of the $1p\frac{1}{2}$ hole is largely inside the nucleus, the effective M/M^* is significantly greater than 1. The Schrödinger-equivalent wave function has a smaller rms radius and consequently the form factor falls off more slowly at high q, in better agreement with the data. As expected from Fig. 5, the core response included automatically in the self-consistent current suppresses the form factor at low q and enhances the form factor above ~ 1 fm^{-1}. Again, the effect is fairly large because the valence hole sees the nuclear interior. Differences in the RPA and self-consistent curves are not surprising because changes in the valence wave function due to self-consistency, even in the $L_{\max}=0$ calculation, can be as large as the subsequent effects from core polarization. In addition, the RPA curve does not include core-polarization contributions to the anomalous current.

Unlike the situation with isoscalar magnetic moments, the M/M^* enhancement of the valence current above 1

TABLE V. Magnetic moments in linear (L) and nonlinear (NL) self-consistent models for nuclei near closed shells are compared to Schmidt moments and to experiment. Moments with the valence nucleon contribution only are for the linear model.

Nucleus	Schmidt	Valence	L	NL	Expt.
^{15}N	−0.264	+0.020	−0.250	−0.285	−0.283
^{15}O	+0.638	+0.667	+0.648	+0.674	+0.179
^{17}O	−1.913	−1.91	−2.03	−2.00	−1.894
^{17}F	+4.793	+5.05	+4.89	+4.87	+4.722
^{39}K	+0.124	+0.855	+0.380	+0.264	+0.391
^{39}Ca	+1.148	+1.17	+0.94	+1.05	+1.022
^{41}Ca	−1.913	−1.91	−2.20	−2.10	−1.595
^{41}Sc	+5.793	+6.41	+6.08	+5.99	+5.430
^{89}Y	−0.264	+0.081	−0.359	−0.376	−0.137
^{91}Zr	−1.913	−1.90	−2.06	−1.99	−1.304
^{207}Pb	+0.638	+0.673	+0.736	+0.745	+0.582
^{209}Bi	+2.624	+5.07	+3.89	+3.45	+4.080

TABLE VI. Magnetic moments in a linear (L) self-consistent model for selected nuclei near closed shells. The moments are decomposed into Dirac and anomalous contributions, and contributions for $L_{max}=0$ and 3 are compared.

Nuclear		Dirac		Anomalous	
		$L_{max}=0$	$L_{max}=3$	$L_{max}=0$	$L_{max}=3$
^{89}Y	core	0.0	−0.289	0.0	−0.418
	valence	+0.714	+0.768	−0.633	−0.421
	total	+0.714	+0.479	−0.633	−0.839
^{91}Zr	core	0.0	−0.22	0.0	+0.06
	valence			−1.90	−1.90
	total	0.0	−0.22	−1.90	−1.84
^{207}Pb	core	0.0	−0.100	0.0	+0.341
	valence			+0.674	+0.495
	total	0.0	−0.100	+0.674	+0.836
^{209}Bi	core	0.0	−1.19	0.0	−0.01
	valence	+6.55	+6.55	−1.48	−1.45
	total	+6.55	+5.36	−1.48	−1.46

fm^{-1} persists after self-consistency is restored. It is also evident that the effect pushes the relativistic predictions away from the data. We note that we can expect significant effects from isovector contributions not included here; for example, nonrelativistic calculations have found strong suppression of the ^{15}N form factor from core polarization, principally because of the tensor component of the residual interaction.[46] However, there is no obvious mechanism that will cancel the relativistic enhancement of the current.

In Fig. 9, we compare predictions of the linear and nonlinear mean-field models for the ^{15}N form factor. The linear model shows greater enhancement due to the core response, in agreement with nuclear matter calculations of the response function in the two models.[27] However, these differences are small compared to the magnitude of the M^* effects (which are significant in both models). We conclude that discrepancies with experiment cannot be attributed to differences in the Hartree wave functions for mean-field models.

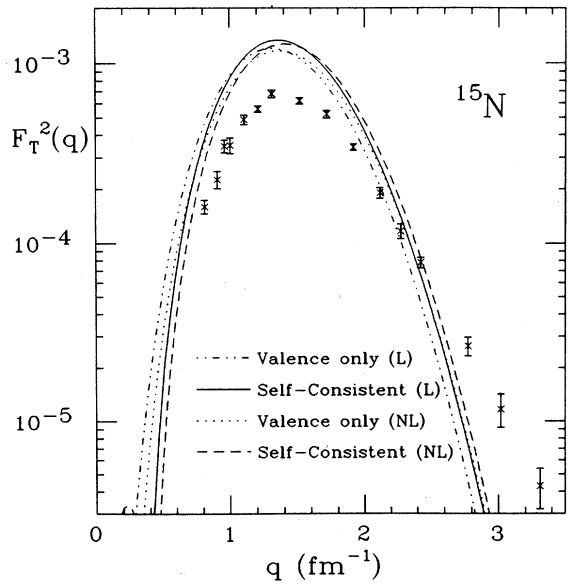

FIG. 9. Elastic magnetic form factor for ^{15}N using the linear and nonlinear parameters from Table I. The curves are the linear model valence only (dot-dashed) and self-consistent (solid), and the nonlinear model valence only (dotted) and self-consistent (dashed).

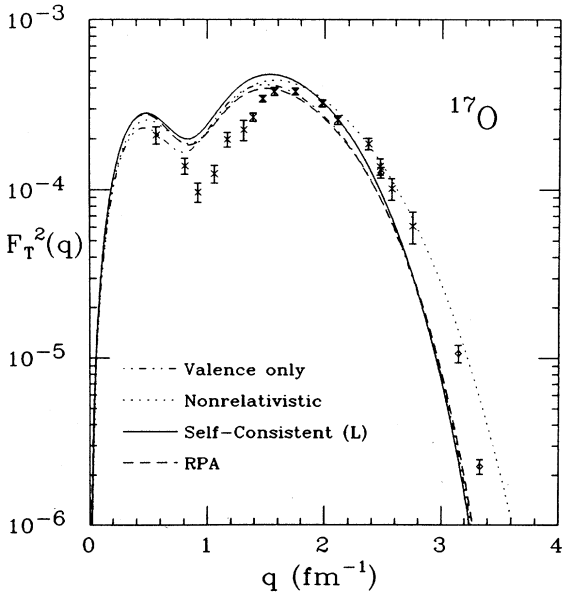

FIG. 10. Elastic magnetic form factor for ^{17}O, using the linear model parameters. The dot-dashed curve is valence only, the dotted curve is a Schrödinger-equivalent calculation, the solid curve is the self-consistent Hartree calculation, and the dashed curve is an RPA calculation from Ref. 27. Experimental data are from Ref. 45.

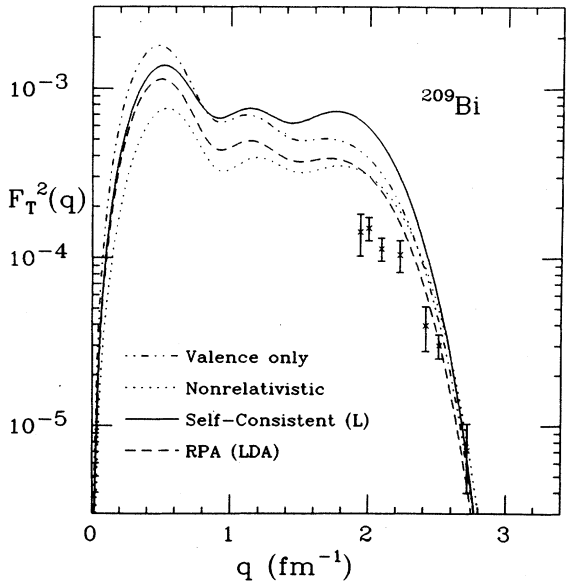

FIG. 11. Elastic magnetic form factor for ^{209}Bi, using the linear parameters from Table I. The dot-dashed curve is valence only, the dotted curve is a Schrödinger-equivalent calculation, the solid curve is the self-consistent Hartree calculation, and the dashed curve is an RPA calculation from Ref. 24.

The form factor for ^{17}O (Fig. 10) shows only slight differences between the valence only and the Schrödinger-equivalent curves below 1 fm^{-1} and the same slower falloff for the nonrelativistic curve. The latter result is again in better agreement with the data. Since ^{17}O is basically a neutron outside a closed shell, the valence convection current does not contribute and only the *correction* to the isoscalar current from the core response is seen. (Differences between the RPA and self-consistent curves are due to wave-function mixing of the valence state and to changes in the anomalous current.) As a result, we find no signatures of relativistic dynamics in this form factor. We note that core polarization and meson exchange effects are important for the $M3$ multipole in nonrelativistic calculations. It will be interesting to see if this is also true in relativistic calculations that include pions.

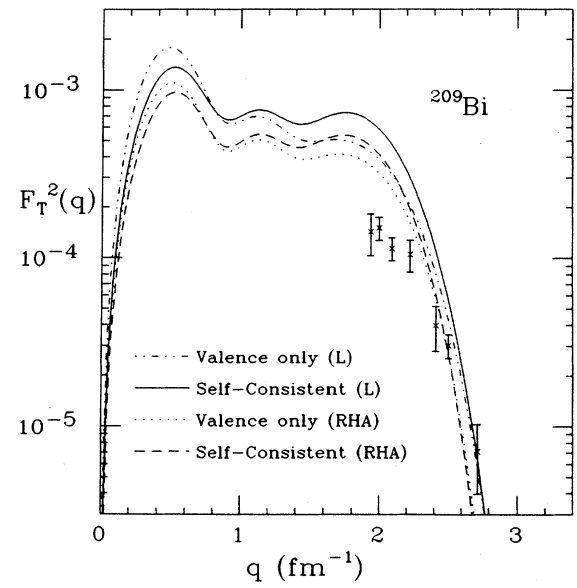

FIG. 12. Elastic magnetic form factor for ^{209}Bi, using the linear and RHA models. The curves are the linear model valence only (dot-dashed) and self-consistent (solid), and the RHA model valence only (dotted) and self-consistent (dashed).

In Fig. 11, the self-consistent $L_{\max}=0$ and 3 form factors for ^{209}Bi are compared to a Schrödinger-equivalent curve and a calculation from Ref. 24 that included the core response to the valence nucleon in a local density approximation (LDA). This LDA only included the part of the response responsible for suppressing the current at low q; it is incorrect at higher q and so the discrepancy between this curve and the $L_{\max}=3$ curve is not surprising. Once again we find enhancement of the $L_{\max}=0$ valence form factor with respect to the nonrelativistic single-particle prediction and further enhancement at moderate q from core polarization. Enhancement is observed in both the Dirac and anomalous currents, and moves the form factor further from experiment.

Results from nuclear matter and calculations in finite nuclei with local density approximations indicate that a one-loop (RHA) model may provide a superior description of relativistic currents.[29] In the first place, the enhancement of the pure valence current is less because M^*/M is closer to 1. Secondly, the nuclear matter response in the RHA is very different from the mean-field theory; virtually no enhancement is predicted for intermediate q. Only the first effect is evident in Fig. 12, where linear MFT and RHA calculations for ^{209}Bi are compared. The RHA core response still enhances the valence current, partly because the present RHA calculation includes the vacuum contributions only in a local density approximation; the vacuum polarization current [Eq. (2.23)] will tend to cancel the enhancement.

IV. DISCUSSION

The results in Sec. III for bulk properties of nuclei provide further evidence that mean-field models can quantitatively describe many properties of finite nuclei, if a nonlinear parameter set is used. The key consequences of adding nonlinearities are the reduction of the surface energy relative to linear parameterization and a slight increase in M^*/M (see Table I), which leads to somewhat less spin-orbit strength.

The successful parameter sets feature negative quartic self-couplings. This implies that the mean-field energy is unbounded, although, in practice, the local minimum is well defined. As discussed in Ref. 10, one can view the nonlinear contributions as a phenomenological adjustment of the density dependence near equilibrium, which simulates higher-order corrections. However, extrapolations of this mean-field model away from the density or energy region of normal nuclear matter are, at best, ques-

tionable. Some implications of negative λ for the nuclear matter equation of state are discussed in Ref. 47.

We have explicitly verified that isoscalar magnetic moments are returned to the Schmidt lines when full self-consistency is restored. All models give the same result and there appears to be no room for signatures of relativistic dynamics. On the other hand, many features of isovector magnetic moments in the mean-field framework remain unexplored. For example, with the assumptions we have made in the present work on the symmetry of the nuclear ground state, the contributions of a neutral pion mean field would not vanish. We could include a pion field with pseudoscalar pion-nucleon coupling by adding the field equation

$$(\nabla^2 - m_\pi^2)\pi^0(\mathbf{x}) = -g_\pi \sum_\alpha^{\text{occ}} \bar{U}_\alpha(\mathbf{x})\tau_3\gamma_5 U_\alpha(\mathbf{x}) \equiv -g_\pi \rho_\pi(\mathbf{x}) , \tag{4.1}$$

and modifying the Dirac Hamiltonian h to h',

$$h \to h' = h + \beta[g_\pi \tau_3 \gamma_5 \pi^0(\mathbf{x})] . \tag{4.2}$$

The pion field expansion analogous to Eq. (2.7) is a sum over odd Legendre polynomials.

Preliminary calculations with pseudoscalar π-N coupling indicate very large effects on magnetic moments in Table V. However, relativistic RPA calculations and other bits of Dirac phenomenology suggest that pseudovector π-N coupling should be used. These considerations for odd-A nuclei have yet to be studied.

While the apparent failure of the relativistic mean-field phenomenology in predicting isoscalar magnetic moments is removed by restoring full self-consistency, problems remain at higher momentum transfers. Unless further corrections generate large cancellations, the enhancements predicted in the mean-field models are not reflected in the elastic magnetic scattering data. The origin of the enhancement is the transverse vector particle-hole interaction (mediated by $\mathbf{V}$), which becomes increasingly attractive as M^* decreases, and even causes an instability of nuclear matter at higher density and intermediate q.[29] In the finite odd-A nucleus, the valence nucleon becomes the source of a vector interaction that causes, through self-consistency, a particle-hole core polarization, which increases the convection current at finite q.

As discussed in Ref. 29, vacuum polarization has major effects on the nuclear response at intermediate q, where the RHA response is very different from the mean-field theory. As a result, the RHA may provide a better phenomenology for currents. RHA models have not been able to reproduce quantitatively all of the nuclear structure successes of the nonlinear mean-field model;[10,48] however, negative quartic couplings have not been considered and may be essential.

We have emphasized the simplicity of the physical picture presented by the relativistic mean-field models but we have pushed their application into regions where they may be difficult to justify. In addition, we have avoided angular momentum projection, pairing, and have included center-of-mass corrections in only the crudest fashion. However, the results are offered without apology. By comparing theoretical and experimental systematics we can evaluate the mean-field physics over a wide range of nuclei without burying the simplicity of the mean-field description. Since an ultimate goal is to provide reliable wave functions and densities for scattering calculations, further evaluations of the approximations are necessary and more sophisticated calculations are likely to be needed.

V. SUMMARY

In this paper, we study the ground-state properties of odd-A nuclei near closed shells in relativistic mean-field models, including both linear and nonlinear parametrizations. The relativistic Hartree equations for the deformed intrinsic ground state are solved using an iterative method based on expanding meson fields and source densities in an angular basis. Pairing correlations are not explicitly included.

For bulk properties (binding energies, rms radii, and quadrupole moments), the extension to odd-A nuclei continues the success found in spherical and even-even nuclei. That is to say, a linear parametrization is deficient in some respects but a nonlinear parametrization can reproduce experimental systematics at the level of the best nonrelativistic Skyrme calculations.

Calculations of convection currents verify the results obtained using a linear response approximation (RPA), including the suppression of the impulse approximation current at low q and enhancement at higher q. The M^* and core response enhancement of the current push predictions for elastic magnetic scattering further from experimental data than predictions from simple nonrelativistic models. Thus, at least for now, this is a failure of the mean-field phenomenology. Hartree calculations including vacuum corrections (RHA) are not expected to exhibit this enhancement and may provide a more consistent model of the current. However, the present calculations only include vacuum effects in a local density approximation and enhancement is still seen.

For all models, isoscalar magnetic moments are found to be close to the Schmidt moments, as expected. Isovector currents and magnetic moments are sensitive to the details of the models and require additional investigation before definite statements can be made. In addition, some nuclei are particularly affected by full self-consistency, possibly highlighting the need for some sort of projection.

Extensions of the present investigations could include the following.

(1) A detailed investigation of the isovector interaction in the Hartree approximation and mean-field phenomenology. This means looking at pseudoscalar versus pseudovector pion-nucleon coupling, tensor-coupled rho mesons, the issue of contact terms, and so on.

(2) An improved treatment of the vacuum corrections in a finite nucleus. In particular, this means incorporating the derivative expansion corrections of Eqs. (2.21) and (2.23).

(3) Extending existing Hartree-Fock calculations of

spherical nuclei to odd-A nuclei.

(4) Exploring the consequences of angular momentum projection and pairing correlations.

ACKNOWLEDGMENTS

We are pleased to thank our colleagues T. Cohen, C. J. Horowitz, J. A. McNeil, E. Rost, B. D. Serot, and J. R. Shepard for many stimulating discussions and constructive criticism. This work was supported in part by the U.S. Department of Energy, Nuclear Physics Division, under Contracts W-31-109-ENG-38, DE-FG02-87ER-40355, and DE-FG05-87ER-40322.

APPENDIX

1. Solving the mean-field equations

In this appendix, we provide details for solving the mean-field equations described in Sec. II. We will discuss the σ-ω model only; extensions to include other mesons are straightforward.

For given source densities, the meson equations (2.2)–(2.4) are solved by integrating over an appropriate Green's function, which is simply a Yukawa function. (If the source density depends on the fields, the procedure is iterated.) For example, the field V_0 is given by

$$g_v V_0(\mathbf{x})=\frac{g_v^2}{4\pi}\int d^3x' \frac{e^{m_v|\mathbf{x}-\mathbf{x}'|}}{|\mathbf{x}-\mathbf{x}'|}\rho_B(\mathbf{x}') \ . \tag{A1}$$

We expand the Yukawa propagator in spherical harmonics and modified Bessel functions

$$\frac{g_i^2}{4\pi}\frac{e^{-m_i|\mathbf{x}-\mathbf{x}'|}}{|\mathbf{x}-\mathbf{x}'|} = \sum_{K=0}^{\infty}\sum_{M_K} f_K^i(x,x')Y^*_{KM_K}(\Omega_x)Y_{KM_K}(\Omega'_x) \tag{A2}$$

with

$$f_K^i(x,x')=g_i^2\frac{I_{K+1/2}(m_i x_<)K_{K+1/2}(m_i x_>)}{(xx')^{1/2}} \ , \tag{A3}$$

and $i=\{s,v\}$. After expanding the fields and source densities, the angular integrals can be performed using standard angular momentum algebra, and then the meson fields are obtained from radial integrals over the appropriate radial source densities

$$\begin{aligned} g_s\phi^L(x)&=\int_0^\infty x'^2dx' f_L^s(x,x')\rho_s^L(x') \ , \\ g_v V_0^L(x)&=\int_0^\infty x'^2dx' f_L^v(x,x')\rho_B^L(x') \ , \\ g_V V^L(x)&=\int_0^\infty x'^2dx' f_L^v(x,x')\mathbf{J}_B^L(x') \ . \end{aligned} \tag{A4}$$

In practice, the numerical integrals are evaluated using Simpson's rule.

Expressions for the radial functions in Eq. (A4) are compactly written after defining the coefficients A_L and B_L, which are simply angular matrix elements

$$\begin{aligned} A_L(\kappa',\kappa,m)&\equiv\left\langle (l'\tfrac{1}{2})j'm \left| \left[\frac{4\pi}{2L+1}\right]^{1/2} Y_{L0} \right| (l\tfrac{1}{2})jm \right\rangle \\ &=(-1)^{m+1/2}[j'][j]\begin{bmatrix} j' & L & j \\ \frac{1}{2} & 0 & -\frac{1}{2}\end{bmatrix}\begin{bmatrix} j' & L & j \\ -m & 0 & m\end{bmatrix} , \end{aligned} \tag{A5}$$

$$\begin{aligned} B_L(\kappa',\kappa,m)&\equiv\langle (l'\tfrac{1}{2})j'm\,|\,\mathbf{Y}^0_{LL1}\cdot\boldsymbol{\sigma}\,|(\bar{l}\tfrac{1}{2})jm\rangle \\ &=\frac{1}{\sqrt{4\pi}}(-)^{j'-m+l'}\sqrt{6}[l'][\bar{l}][j][j'][L]^2\begin{Bmatrix} l' & \bar{l} & L \\ \frac{1}{2} & \frac{1}{2} & 1 \\ j' & j & L\end{Bmatrix}\begin{bmatrix} j' & L & j \\ -m & 0 & m\end{bmatrix}\begin{bmatrix} l' & L & \bar{l} \\ 0 & 0 & 0\end{bmatrix} , \end{aligned} \tag{A6}$$

where $\bar{l}=2j-l$ is the orbital angular momentum for the lower component and $[j]\equiv\sqrt{2j+1}$. Then the source densities are given by sums over radial wave functions and the A and B coefficients,

$$\begin{aligned} \rho_s(\mathbf{x})&\equiv\sum_{L\ \text{even}}^{L_{\max}} P_L(\cos\theta)\rho_s^L(r) \\ &=\sum_{L\ \text{even}}^{L_{\max}} P_L(\cos\theta)\left[\frac{2L+1}{4\pi r^2}\right]\sum_{\alpha\kappa'\kappa}^{\text{occ}}[G_{\alpha\kappa'}(r)G_{\alpha\kappa}(r)-F_{\alpha\kappa'}(r)F_{\alpha\kappa}(r)]A_L(\kappa',\kappa,m) \ , \end{aligned} \tag{A7}$$

$$\begin{aligned} \rho_B(\mathbf{x})&\equiv\sum_{L\ \text{even}}^{L_{\max}} P_L(\cos\theta)\rho_B^L(r) \\ &=\sum_{L\ \text{even}}^{L_{\max}} P_L(\cos\theta)\left[\frac{2L+1}{4\pi r^2}\right]\sum_{\alpha\kappa'\kappa}^{\text{occ}}[G_{\alpha\kappa'}(r)G_{\alpha\kappa}(r)+F_{\alpha\kappa'}(r)F_{\alpha\kappa}(r)]A_L(\kappa',\kappa,m) \ , \end{aligned} \tag{A8}$$

$$\mathbf{J}_B(\mathbf{x}) \equiv i \sum_{L \text{ odd}}^{L_{\max}} \mathbf{Y}_{LL1}^{M=0*}(\Omega_x) \mathbf{J}_B^L(r)$$
$$= i \sum_{L \text{ odd}}^{L_{\max}} \mathbf{Y}_{LL1}^{M=0*}(\Omega_x) \frac{1}{r^2} \sum_{\alpha\kappa'\kappa}^{\text{occ}} [2G_{\alpha\kappa'}(r) F_{\alpha\kappa}(r)] B_L(\kappa', \kappa, m) \, . \tag{A9}$$

The m label on the radial wave functions has been suppressed in Eqs. (A7)–(A9).

The Dirac equations for the radial wave functions are obtained by substituting the relevant expansions into the full Dirac equation (2.5) and projecting

$$\left[\frac{d}{dr} + \frac{\kappa}{r} \right] G_{\kappa m}^{\alpha}(r) - (M + \epsilon_\alpha) F_{\kappa m}^{\alpha}(r) + \sum_{\kappa'} \sum_{L \text{ even}}^{L_{\max}} A_L(\kappa, \kappa', m) [g_s \phi^L(r) + g_v V_0^L(r)] F_{\kappa' m}^{\alpha}(r)$$
$$- \sum_{\kappa'} \sum_{L \text{ odd}}^{L_{\max}} B_L(\kappa, \kappa', m) [g_v V^L(r)] G_{\kappa' m}^{\alpha}(r) = 0 \, , \tag{A10}$$

$$\left[\frac{d}{dr} - \frac{\kappa}{r} \right] F_{\kappa m}^{\alpha}(r) - (M - \epsilon_\alpha) G_{\kappa m}^{\alpha}(r) + \sum_{\kappa'} \sum_{L \text{ even}}^{L_{\max}} A_L(\kappa, \kappa', m) [g_s \phi^L(r) - g_v V_0^L(r)] G_{\kappa' m}^{\alpha}(r)$$
$$+ \sum_{\kappa'} \sum_{L \text{ odd}}^{L_{\max}} B_L(\kappa, \kappa', m) [g_v V^L(r)] F_{\kappa' m}^{\alpha}(r) = 0 \, . \tag{A11}$$

The assumption that the valence nucleon is placed in a definite m state restricts the expansion of the current (by parity) to $\mathbf{Y}_{LL1}^{M=0}$ terms with odd L. This also ensures current conservation since $\nabla \cdot \phi(r) \mathbf{Y}_{LL1}^{M}(\Omega) = 0$ for any radial function $\phi(r)$.

The mean-field equations are solved by an iterative procedure similar to that described in Ref. 9. Specifically, the radial equations for the orbitals [Eqs. (A10) and (A11)] are solved as coupled-channels equations, by repeatedly integrating the differential equations with appropriate boundary conditions in each component. An inward-outward integration is performed with a fourth-order Runge-Kutta method, and the eigenvalue is obtained by insisting that the full solution (obtained from the superposition of the solutions with boundary conditions imposed on the individual components) be continuous at a prescribed matching radius. Once new wave functions are determined, the boson equations are solved by integrating the source terms over the corresponding Green's functions, as described above. The procedure is continued until self-consistency is achieved, as measured by the change in energy and moments of the density and current with each iteration. Two codes, based on the same approach but written independently, were used to minimize programming and input errors and to ensure that the lowest energy solutions were found.

2. Reduced matrix elements

To facilitate comparisons with Ref. 27, we write the expansion of the baryon current $\mathbf{J}_B$ [Eq. (A9)] as

$$\mathbf{J}_B(\mathbf{x}) = \frac{i}{x^2} \sum_{J \text{ odd}} \left[(-1)^{j_v - m_v} \begin{pmatrix} j_v & J & j_v \\ -m_v & 0 & m_v \end{pmatrix} \right] \times b_J(x) \mathbf{Y}_{JJ1}^{0*}(\Omega_x) \, , \tag{A12}$$

which defines the radial function $b_J(x)$ that is plotted in Fig. 6. Here j_v and m_v refer to the quantum numbers of the valence nucleon, which is assumed to be dominated by a single component in the expansion of the single-particle wave function. We have included the factor in brackets so that b_J will correspond to an (approximate) reduced matrix element of the current.

The reduced matrix element of $\hat{T}_{JM}^{\text{mag}}(q)$ [Eq. (2.15)], with the isoscalar baryon current only, is given by

$$\langle J_i \| \int d^3x \, j_J(qx) \mathbf{Y}_{JJ1}(\Omega) \cdot \mathbf{J}_B(\mathbf{x}) \| J_i \rangle = i \int_0^\infty dx \, j_J(qx) b_J(x) \equiv i \tilde{b}_J(q) \, , \tag{A13}$$

which defines the function $\tilde{b}_J(q)$ plotted in Fig. 6. The function $\tilde{c}_J(q)$ for the isoscalar anomalous current, plotted in Fig. 7, is defined analogously starting from Eq. (2.18).

Note that $\mathbf{J}_B(\mathbf{x})$ is only approximately the matrix element of the current in a state of definite J_i since the self-consistent odd-A solution is a deformed intrinsic state. In principle, one should project out states of good J to calculate the matrix elements for electron scattering, although consistent and unambiguous angular momentum projection techniques for relativistic models have yet to be developed. Approximate projection methods used in nonrelativistic calculations should be applied to the relativistic problem to estimate the size of corrections.

*Present address: Department of Physics, University of Colorado, Boulder, CO 80309.
[1]B. D. Serot and J. D. Walecka, Adv. Nucl. Phys. **16**, 1 (1986).
[2]L. D. Miller, Ann. Phys. (N.Y.) **91**, 40 (1975).
[3]C. J. Horowitz and B. D. Serot, Nucl. Phys. **A368**, 503 (1981).
[4]J. Boguta and A. R. Bodmer, Nucl. Phys. **A292**, 413 (1977).
[5]P.-G. Reinhard, M. Rufa, J. Maruhn, W. Greiner, and J. Friedrich, Z. Phys. A **323**, 13 (1986).
[6]L. G. Arnold, B. C. Clark, R. L. Mercer, and P. Schwandt, Phys. Rev. C **23**, 1949 (1981), and references cited therein.
[7]W. Pannert, P. Ring, and J. Boguta, Phys. Rev. Lett. **59**, 2420 (1988).
[8]S. J. Lee *et al.*, Phys. Rev. Lett. **57**, 2916 (1986); **59**, 1171 (1987).
[9]C. E. Price and G. E. Walker, Phys. Rev. C **36**, 354 (1987).
[10]R. J. Furnstahl, C. E. Price, and G. E. Walker, Phys. Rev. C **36**, 2590 (1987).
[11]Y. K. Gambhir and P. Ring, Phys. Lett. B **202**, 5 (1988).
[12]Some of the magnetic moment results given in Sec. III have been discussed earlier in Refs. 13–16. There are also recent calculations by Ring and collaborators on magnetic moments in a self-consistent odd-A model (using a different calculational method), as reported in Ref. 17.
[13]R. J. Furnstahl, in *Spin Observables of Nuclear Probes,* edited by C. Horowitz, C. D. Goodman, and G. E. Walker (Plenum, New York, 1988).
[14]C. E. Price, in *Spin Observables of Nuclear Probes,* edited by C. Horowitz, C. D. Goodman, and G. E. Walker (Plenum, New York, 1988).
[15]R. J. Furnstahl, in *Relativistic Nuclear Many-Body Physics,* edited by B. C. Clark, R. J. Perry, and J. P. Vary (World Scientific, New Jersey, 1989).
[16]C. E. Price, in *Relativistic Nuclear Many-Body Physics,* edited by B. C. Clark, R. J. Perry, and J. P. Vary (World Scientific, New Jersey, 1989).
[17]U. Hofmann and P. Ring, Phys. Lett. B **214**, 367 (1988).
[18]C. Lederer, J. M. Hollander, and I. Perlman, *Table of Isotopes* (Wiley, New York, 1967).
[19]T. Matsui, Nucl. Phys. **A370**, 365 (1981).
[20]W. Bentz, A. Arima, H. Hyuga, K. Shimizu, and K. Yazaki, Nucl. Phys. **A436**, 593 (1985).
[21]H. Kurasawa and T. Suzuki, Phys. Lett. **165B**, 234 (1986).
[22]G. E. Brown, in *Nuclear Structure at High Spin, Excitation, and Momentum Transfer (McCormick's Creek State Park, Bloomington, Indiana),* Proceedings of the Workshop on Nuclear Structure at High Spin, Excitation and Momentum Transfer, AIP Conf. Proc. 142, edited by Hermann Nann, (AIP, New York, 1986), p. 5.
[23]J. A. McNeil, R. D. Amado, C. J. Horowitz, M. Oka, J. R. Shepard, and D. A. Sparrow, Phys. Rev. C **34**, 746 (1986).
[24]R. J. Furnstahl and B. D. Serot, Nucl. Phys. **A468**, 539 (1987).
[25]S. Ichii, W. Bentz, A. Arima, and T. Suzuki, Phys. Lett. B **192**, 11 (1987).
[26]J. R. Shepard, E. Rost, C.-Y. Cheung, and J. A. McNeil, Phys. Rev. C **37**, 1130 (1988).
[27]R. J. Furnstahl, Phys. Rev. C **38**, 138 (1988).
[28]S. Ichii *et al.*, Nucl. Phys. **A487**, 493 (1988).
[29]C. J. Horowitz, in *Spin Observables of Nuclear Probes,* edited by C. Horowitz, C. D. Goodman, and G. E. Walker (Plenum, New York, 1988).
[30]W. Koepf and P. Ring, Phys. Lett. B **212**, 397 (1988).
[31]A. R. Edmonds, *Angular Momentum in Quantum Mechanics* (Princeton University Press, Princeton, 1960).
[32]B. D. Serot, Phys. Lett. **107B**, 263 (1981).
[33]T. W. Donnelly and J. D. Walecka, Annu. Rev. Nucl. Sci. **25**, 329 (1975).
[34]R. J. Perry, Phys. Lett. B **182**, 269 (1986).
[35]David A. Wasson, Caltech report, 1988.
[36]We expect that the set from Ref. 5 would yield similar predictions to set NL. However, no attempt was made to optimize the nonlinear set; adjustments could undoubtedly improve the results discussed in this section.
[37]H. C. Lee and R. Y. Cusson, Ann. Phys. (N.Y.) **72**, 353 (1972).
[38]K.-H. Passler, Nucl. Phys. **A257**, 253 (1976).
[39]D. Vautherin, Phys. Rev. C **7**, 296 (1973).
[40]H. de Vries, C. W. de Jager, and C. de Vries, At. Data Nucl. Data Tables **36**, 495 (1987).
[41]K. Shimizu, M. Ichimura, and A. Arima, Nucl. Phys. **A226**, 282 (1974).
[42]R. H. Spear, Phys. Rep. **73**, 369 (1981).
[43]G. H. Fuller and V. W. Cohen, Nucl. Data **A5**, 433 (1969).
[44]R. P. Singhal *et al.*, Phys. Rev. C **28**, 513 (1983).
[45]N. Kalanter-Nayestanaki *et al.*, MIT report, 1987.
[46]T. Suzuki, H. Hyuga, A. Arima, and K. Yazaki, Nucl. Phys. **A358**, 421 (1981).
[47]B. M. Waldhauser, J. A. Maruhn, H. Stöcker, and W. Greiner, Phys. Rev. C **38**, 1003 (1988).
[48]W. Fox, Nucl. Phys. **A495**, 463 (1989).